

Seismic microzoning from synthetic ground motion parameters: case study, Santiago de Cuba

Leonardo Alvarez^{a,b,*}, Franco Vaccari^{b,c}, Giuliano F. Panza^{b,c}, Ramón Pico^d

^aCentro Nacional de Investigaciones Sismológicas (CENAI), Caja Postal 2775, Habana13, Cuba

^bThe Abdus Salam International Centre for Theoretical Physics (ICTP), Strada Costiera No. 11, Trieste 34014, Italy

^cDipartimento di Scienze della Terra, Università di Trieste (DST), Via Weiss No. 4, Trieste 34127, Italy

^dInstituto de Cibernética, Matemática y Física (ICIMAF), E No. 309, e/13 y 15, Vedado, C.Habana, CP 10400, Cuba

Accepted 14 February 2005

Abstract

Synthetic seismograms (P-SV and SH waves) have been calculated along six profiles in Santiago de Cuba basin, with a cutoff frequency of 5 Hz, by using a hybrid approach (modal summation for a regional 1D structure plus finite differences for a local 2D structure embedded in the first). They correspond to a scenario earthquake of $M_S=7$ that may occur in Oriente fault zone, directly south of the city. As initial data for a seismic microzoning, the characterisation of earthquake effects has been made considering several relative (2D/1D) quantities (PGDR, PGVR, PGAR, DGAR, I_{AR} —ratios of peak ground values of displacement, velocity and acceleration, and of design ground acceleration and Arias intensity-, etc.) and functions representative of the ground motion characteristics in soil (2D) with respect to bedrock (1D). The functions are the response spectra ratio $RSR(f)$, already routinely used in this kind of work, and the elastic energy input ratio $E_I R(f)$, defined, for the first time, in this paper. These data, sampled at 115 sites within all the profiles have been classified in two steps, using logical combinatory algorithms: connected components and compact sets. In the first step, from the original ground motion parameters or functions extracted from the synthetic seismograms, nine sets have been classified and the partial results show the spatial distribution of the soil behaviour as a function of the component of motion. In the second step, the results of the classification of the nine sets have been used as input for a further classification that shows a spatial distribution of sites with a quasi-homogeneous integral ground motion behaviour. By adding the available geological surface data, a microzoning scheme of Santiago de Cuba basin has been obtained.

© 2005 Published by Elsevier Ltd.

Keywords: Synthetic seismograms; Ground motion parameters and functions; Seismic microzoning; Classification

1. Introduction

Seismic microzoning was introduced in seismological practice more than 40 years ago. The use of microtremors for estimating some characteristics of foundation soils dates from the fifties [1]. The classical book of Medvedev [2] summarises the results of Soviet scientist's initial experiences in that discipline. They first used the value ΔI as a parameter for microzoning. This value is defined as the increment (or decrement) of the expected macroseismic intensity over the one corresponding to a 'reference soil', in which the macroseismic intensity predicted by regional

seismic hazard assessment ('base degree') is expected to occur. The data used for that purpose are, first of all, of engineering-geological character, complemented with microseisms' and/or microearthquakes' measurements. Further development of the Soviet school on seismic microzoning, due to the fact that building codes were prepared always in terms of macroseismic intensity, was directed to the upgrading of the methods to calculate ΔI , as a basis of a microzoning map, complemented with the analysis of the spectral behaviour of soils through transfer functions calculated by different methods [3,4].

In western countries, this kind of work began later and followed a different path. Seismic hazard was mainly estimated in terms of peak acceleration values, and microzoning was directed to the estimation of relative amplification (a transfer function) of expected ground motion with respect to a point (believed to represent the bedrock), the 'reference site' [5–7].

* Corresponding author

E-mail address: leovalvar@ictp.trieste.it (L. Alvarez).

Another variant, widespread in present times, was the spectral ratio method [8], that considers the Earth as a simple two-layer model (sediments over bedrock) and assumes that the ratio of horizontal to vertical component of microseisms can be related to the transfer function of S waves. Although the use of this method is very popular, there are serious objections to its validity [9].

The key point in the microzoning studies is to determine what is a ‘reference soil’ for ΔI calculation, or a ‘reference site’ for transfer function evaluation, which is not a simple process. In the case of the ‘reference soil’ the procedure can be divided in two parts: (a) to identify a kind of soil, present in the area of study, that is consistent with the regional hazard estimation, (b) in the area covered by this kind of soil, to select a point or a group of points, considered ‘characteristics’ of this soil, which can be used as reference for some relative calculations of microseisms’ or micro-earthquakes’ measurements, of acoustic impedance, etc. In the case of the ‘reference site’ the problem is to find a site that can be considered as bedrock, to be used for the definition of the transfer functions of sedimentary layers.

Modelling is a way to avoid this problem. If the regional structure is known, it is possible to obtain realistic synthetic seismograms for the bedrock model, and if the local structure is known, realistic synthetic seismograms can be obtained for different ground conditions. Then, microzoning can be achieved by comparison of these two kind of synthetic seismograms. For this purpose, ground motion parameters should be extracted first. This procedure has been applied to the city of Rome [10]; an a-priori geotechnical zonation is used as a basis for a ground motion characterisation, in terms of response spectra ratio (RSR) and other parameters pertinent for the seismic microzoning. Another variant has been applied by Alvarez et al. [11], who made the microzonation by classifying the RSR curves calculated at sites distributed over the city plain, using geological data as auxiliary for the tracing of the borders between different zones. The theoretical principles of this methodology are presented by Panza et al. [12], and the results obtained in applying these principles to the seismic microzoning of 14 cities worldwide are summarised in Ref. [13].

The purpose of this paper is to make a microzoning, through a classification procedure of several relative ground motion quantities, extracted from synthetic seismograms. The flow chart of the microzonation procedure is shown in Fig. 1. The synthetic signals in the bedrock anelastic structure are generated by the modal summation approach [13–16]. The waveforms along the local, laterally varying anelastic structure are computed using a finite difference scheme applied to the local structure, combined with modal summation [17,18]. This procedure is known as the ‘hybrid approach’. The case study is Santiago de Cuba, one of the first cities founded by Spanish in America (1508), on the south-eastern coast of Cuba island (in a protected deep water bay), that is exposed to a moderate to high seismic hazard. The first report of a felt earthquake is from 1578,

and from its foundation to the present day it had experienced five shakings of intensity VIII and two of intensity IX in the MSK scale (equivalent to MMI and EMS scales for those intensities). From the macroseismic data, the magnitudes of these earthquakes have been estimated between 6.8 and 7.6. These values together with the low magnitude earthquakes in the Oriente fault zone give a good basis to consider a scenario earthquake of magnitude 7, south of the city, at about 30 km distance off the coast [19]. The city has been the object of several microzoning studies, using classical Soviet school methodology [20,21] and some GIS based methodological variants [22,23], as well as modelling of P-SV and SH waves [11,19].

2. Ground motion parameters

The target of seismic microzoning is to represent in a map the relative variation of the expected seismic ground motion as a function of soil conditions.

In earthquake engineering, values of peak ground displacement (PGD), velocity (PGV) and acceleration (PGA), design ground acceleration (DGA) and Arias intensity (I_A) are often used among others. For all these quantities (generally indicated with X in Eq. (1)) it is possible to calculate the ratio, XR, between the values computed in the laterally varying medium, X_{2D} , and these computed in the bedrock model X_{1D} :

$$XR = X_{2D}/X_{1D} \quad (1)$$

We will consider the cases $XR = (PGDR, PGVR, PGAR, DGAR, I_AR)$.

The use of the elastic response spectra ratio (RSR), a function defined as:

$$RSR(f) = RS_{2D}(f)/RS_{1D}(f) \quad (2)$$

where RS_{2D} and RS_{1D} are the elastic response spectra (5% damped), of the 2D and 1D signals, respectively, calculated for a viscous damping of 5%, has been proved to be very useful for microzoning purposes [10,11,13].

In the 90’s in earthquake engineering it has been introduced the use of the earthquake input energy spectrum (E_1), a function defined as:

$$\frac{E_1(T, \nu, \mu)}{m} = \int \ddot{u}_t du_g = \int \ddot{u}_t \dot{u}_g dt \quad (3a)$$

where u_g is the input seismogram (i.e. the earthquake ground displacement), u_t is the absolute displacement $u_t(t) = u(t) + u_g(t)$, and $u(t)$ is the solution of the single degree of freedom (SDOF) problem under the action of an earthquake input u_g [24,25]. The structure is characterised by the viscous damping constant ν , the displacement ductility μ , the oscillation period T and the mass m . In the following E_1/m will be called E_1 , like in [24,25]. This function, for a viscous damping of 5%, is plotted in the (T, E_1) plane and a new

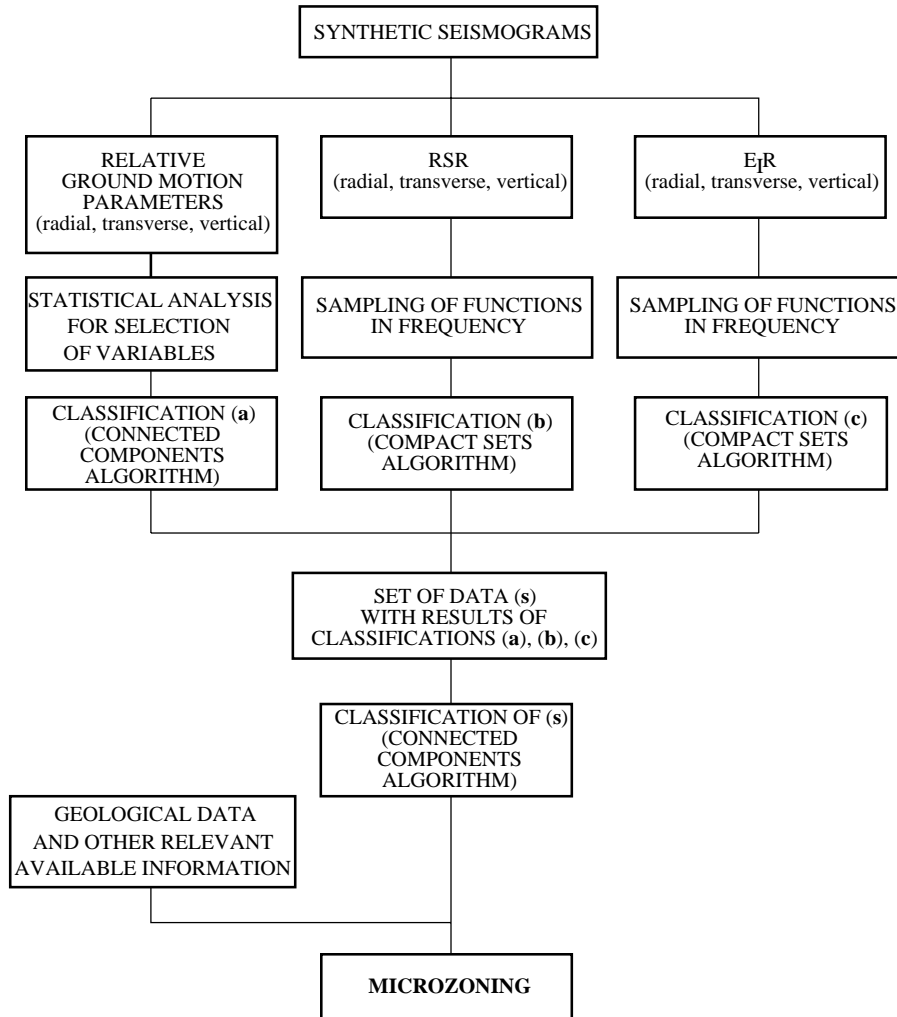


Fig. 1. Flow-chart of the microzonation procedure.

variable (AE_1) is defined: the area enclosed by the elastic input energy spectrum in the interval of periods between 0.05 and 4.0 s.

$$AE_1 = \int_{0.05}^{4.0} E_1(\nu = 5\%, T) dT \quad (3b)$$

Eqs. (3a) and (3b), may be considered a global hazard index in energy terms [25] as it considers the influence of the energy demand in the whole period range, and have been successfully used for the characterisation of site-dependent seismic hazard [26]. The value of μ separates two different cases, the elastic ($\mu = 1$), for which symbols E_1 and AE_1

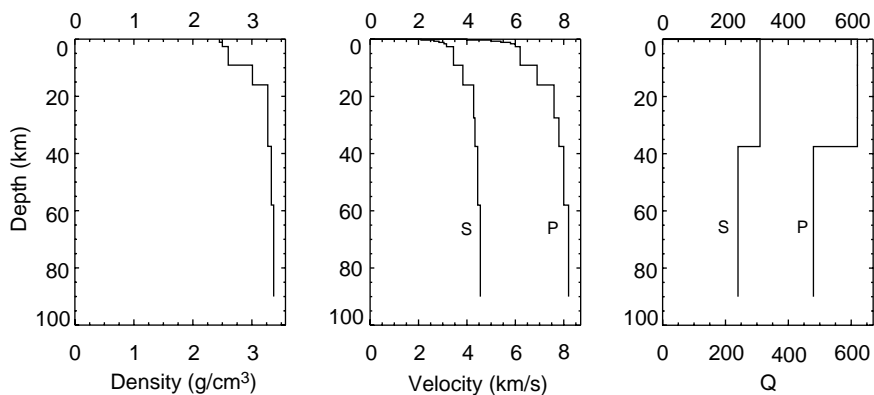


Fig. 2. Regional structural model.

are used and the anelastic ($\mu > 1$), that is expressed trough $E_I\mu$ and $AE_I\mu$ [27]. Let us define a new function, the elastic earthquake input energy spectra ratio (E_1R):

$$E_1R(f) = E_{I2D}(f)/E_{I1D}(f) \tag{4}$$

where E_{I2D} and E_{I1D} are the mean elastic earthquake input energy spectra (E_I) for the laterally varying structure and the bedrock model, respectively. The use of the frequency,

instead of the period that appears in the definition (3a), makes possible the direct comparison of $E_1R(f)$ with $RSR(f)$.

Additionally, we can define AE_1R , i.e. the ratio between the areas under the curves of E_I :

$$AE_1R = AE_{I2D}/AE_{I1D} \tag{5}$$

where AE_{I2D} and AE_{I1D} are the corresponding values of the areas under the curves of E_I for the laterally varying structure and the bedrock model, respectively.

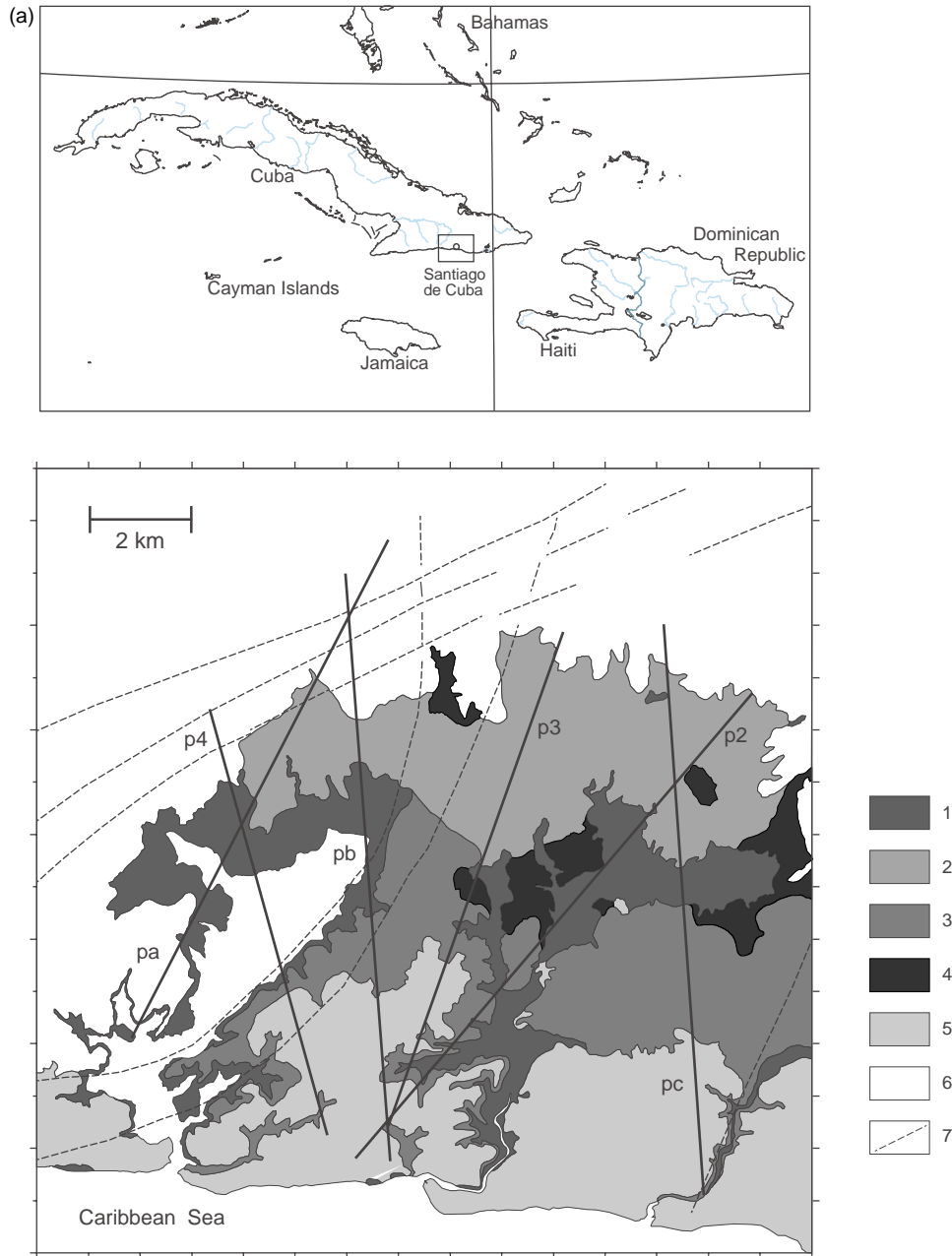


Fig. 3. (a) Profiles traced over a simplified geological scheme of Santiago de Cuba basin (modified from [32]), 1—sand and sandstones (Quaternary formations), 2—clays (Neogene), 3—marls (Neogene), 4—magmatic intrusions, 5—calcareous rocks and limestones (Neogene and Quaternary formations), 6—rocks from El Cobre formation (Paleogene Volcanic Arc), 7—faults. The ticks on the frame of the figure are 1 km apart, the left-low corner has coordinates 19.945°N. and 75.897°W.; (b) Cross sections of the profiles. The numbering in the legend corresponds to different kind of soils, whose mechanical parameters are given in Table 1.

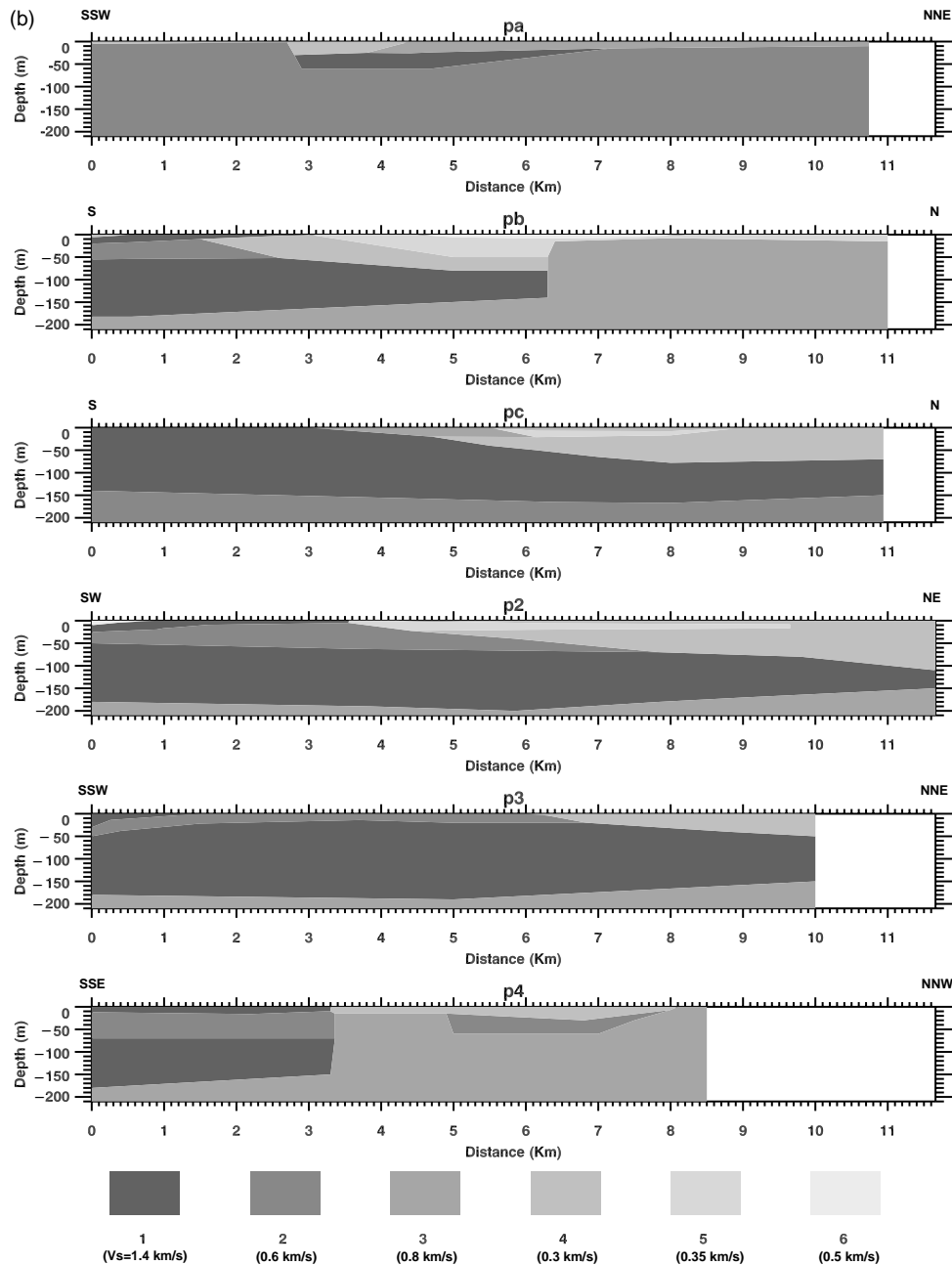


Fig. 3 (continued)

3. Data

The regional structure model (until 110 km of depth) has been constructed, using results of geophysical studies [28,29] and tomographic inversions [30,31] (Fig. 2), and it has been used to calculate the bedrock P-SV and SH waves seismograms by modal summation to a maximum frequency of 10 Hz. Six 2D profiles, that cross the entire basin where Santiago de Cuba is located, have been constructed using borehole data. In Fig. 3a their traces are shown over

a simplified version of the geological map of Medina et al. [32] of Santiago de Cuba basin. In Fig. 3b the corresponding cross-sections are shown. The data about the mechanical properties (P- and S- waves velocities and quality factors) of the strata (see Table 1) were taken from the literature [4, 33,34], and correspond to direct measurements made on similar soils in other places in Cuba, as no local measurements are available. A brief discussion about the geological setting of Santiago de Cuba basin and the data about its subsurface geology can be found in Refs. [11,19].

Table 1
Values of the mechanical parameters of the strata present in the profiles

Code	ρ (g/cm ³)	v_P (km/s)	Q_P	v_S (km/s)	Q_S
1	2.3	2.5	200	1.4	100
2	2.0	1.3	150	0.6	50
3	2.1	2.4	350	0.8	15
4	1.6	0.8	100	0.3	50
5	1.8	1.2	100	0.35	50
6	1.8	0.9	150	0.5	50

The code corresponds to numbers in the legend of Fig. 3b. ρ —density, v_P , v_S —velocities of P and S waves, Q_P , Q_S —quality factors of P and S waves.

4. Synthetic seismograms and derived parameters

The complete set of seismograms of P-SV and SH-waves for displacement, velocity and acceleration have been computed, at sites along the six profiles, by the hybrid approach [17,18] considering a maximum frequency of 5 Hz. Along each profile, the sites are on the free surface, with a constant spacing of 180 m. We considered a point source with seismic moment $M_0 = 1.0 \times 10^{13}$ Nm (characterised by a flat spectrum in the range of frequencies used), focal depth $h = 20$ km, and focal mechanism: dip = 21°, azimuth = 100° and rake = 21°. This mechanism is a combination of left-lateral strike slip with normal faulting, characteristic of this zone, and gives the maximum energy radiation in the direction of the studied profiles. The computations were made twice, once considering the complex 2D structures, formed by the regional structure and the embedded in it detailed 2D profiles, and the second considering the uniform bedrock model only. As it was pointed out in the introduction, this dual calculation is important for microzoning purposes, because it allows us to calculate the variations of the earthquake ground motion, relative to the bedrock, i.e. the real site increment against the reference site. In our case, we do not have the quite common problem of selecting the reference site, because it is formed by the rock basement. The ‘elementary’ seismograms have been scaled, in the frequency domain [35], for the scenario earthquake of magnitude ($M_S = 7$) by using the scaling law of Gusev [36], as reported by Aki [37]. The design ground acceleration (DGA) is obtained following the procedure defined by Panza et al. [35] using the design response spectra of the Cuban building code [38] for soils of type S1. The scaled seismograms (e.g. see Fig. 4) have been used for calculating the earthquake input energy spectrum E_I and the corresponding AE_I that turn out to be a little underestimated, since our integral begins at $T = 0.2$ s. instead of 0.05 s, as defined in (3b). Nevertheless, since we are interested in relative values, our choice of the integration interval does not affect our conclusions.

All the above defined relative quantities plus the maximum values of the functions RSR and $E_I R$ (RSR_{\max} , $E_I R_{\max}$) and the frequencies at which these maxima occur [$f(RSR_{\max})$, $f(E_I R_{\max})$] have been plotted for each profile

(an example is given in Fig. 5). Additionally we have drawn the plots of the functions $RSR(f, x)$ and $\log[E_I R(f, x)]$ where ‘ x ’ is the epicentral distance to the site, formed by the original $RSR(f)$ and $E_I R(f)$ evaluated in each of the sites considered. Examples are shown in Fig. 6 for RSR (together with the profile structure plot) and Fig. 7 for $\log[E_I R]$.

5. Ground motion parameters classification

5.1. Single valued parameters

The data shown in Fig. 5 correspond to the entire site set along profile p3 (see Fig. 3a) where the synthetic seismograms have been calculated (radial component). The same has been done for all the profiles, for a total of 352 sites, and for the three components of motion. Since we do not observe, in general, a high variability of the curves, like the ones given in Fig. 5, in nearby sites, we decided, without a significant loss of information, to decimate (every three points) the available sites, which resulted in 115 sites, 560 m apart, along the profiles. In the following, the analysis will be limited to the decimated set of signals.

The data for the 10 single-valued ground motion parameters [PGDR, PGVR, PGAR, DGAR, I_{AR} , RSR_{\max} , $E_I R_{\max}$, $AE_I R$, $f(RSR_{\max})$, $f(E_I R_{\max})$] have been divided into three sets, one for each component of motion, P-SV vertical, P-SV radial and SH (transverse). In order to select the variables to be used in the classification, a non-parametric correlation analysis between the different ground motion parameters has been made for each set. Because of the high values of $E_I R_{\max}$ present in the vertical component, its logarithm is used. The Spearman rank-order correlation and the Kendall’s τ were tested. The hypothesis of independence of variables is rejected for all combinations of variables except when at least one of the variables is $f(RSR_{\max})$ or $f(E_I R_{\max})$ for the radial and transverse components, at a significance level of 10^{-4} . The above is also true for the vertical component, and in addition the hypothesis of independence with respect to all other variables holds for $\log(E_I R_{\max})$ and $AE_I R$ too. This is a consequence of the presence of some isolated very high values of these variables (outliers) and we decided not to take them into account because they don’t allow a clear classification. With this exception, we have only three really independent variables that can be used for classification: the frequencies of the maxima of $f(RSR_{\max})$ and $f(E_I R_{\max})$, and one of the remaining eight, let’s say, the maximum velocity ratio PGVR. Three sets of values are formed, one for each of the ground motion components.

5.2. $RSR(f)$ and $E_I R(f)$ functions

In a previous paper [11] the classification of the function $RSR(f)$ for the transverse component at $f_{\max} = 1$ Hz along four profiles have been used for microzoning

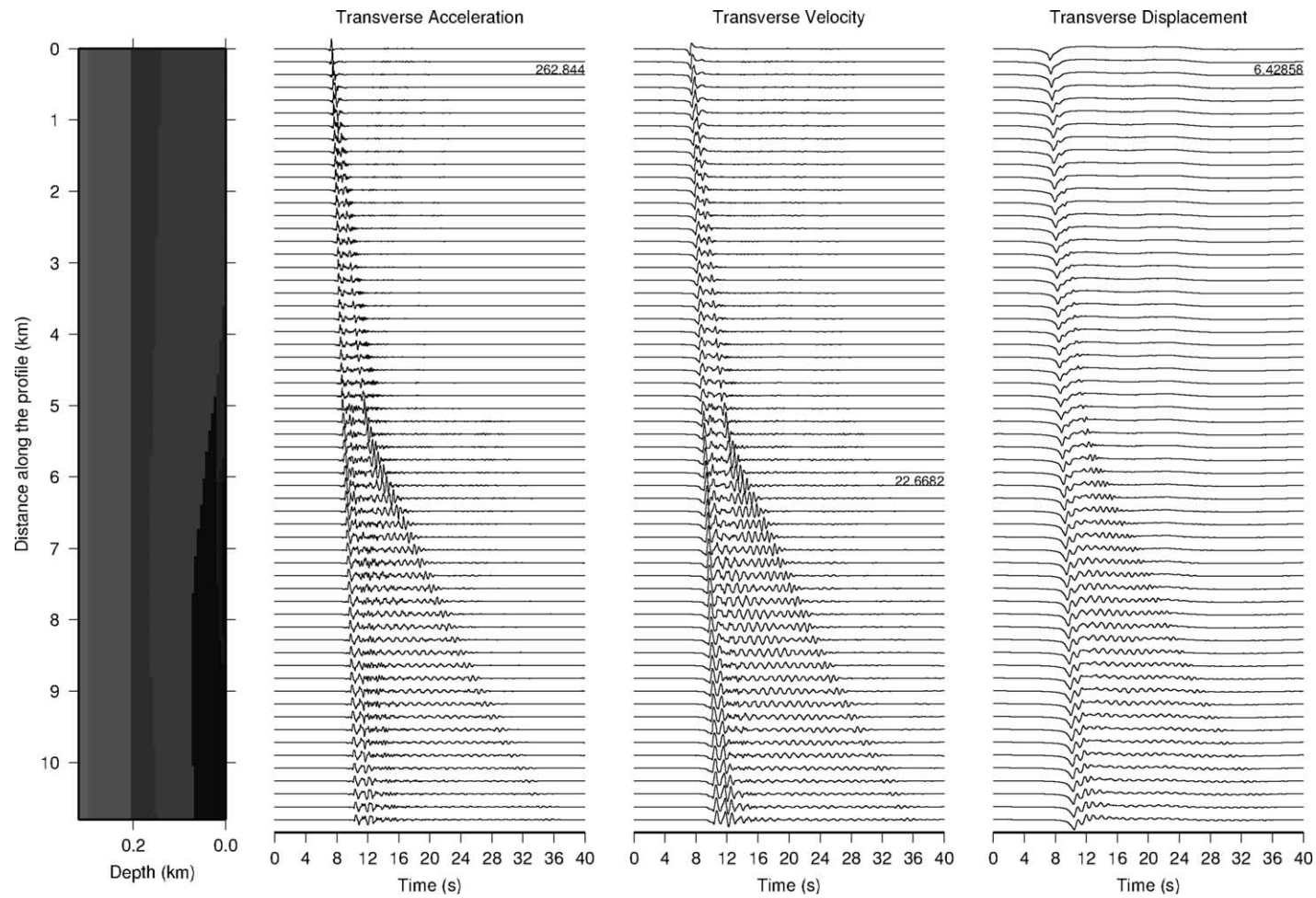


Fig. 4. Example of synthetic signals for a scenario earthquake of $M_S=7$ at a distance of about 30 km from the beginning of the profile (the one labelled as 'pc' in Fig. 3a and b), and at a depth of 20 km.

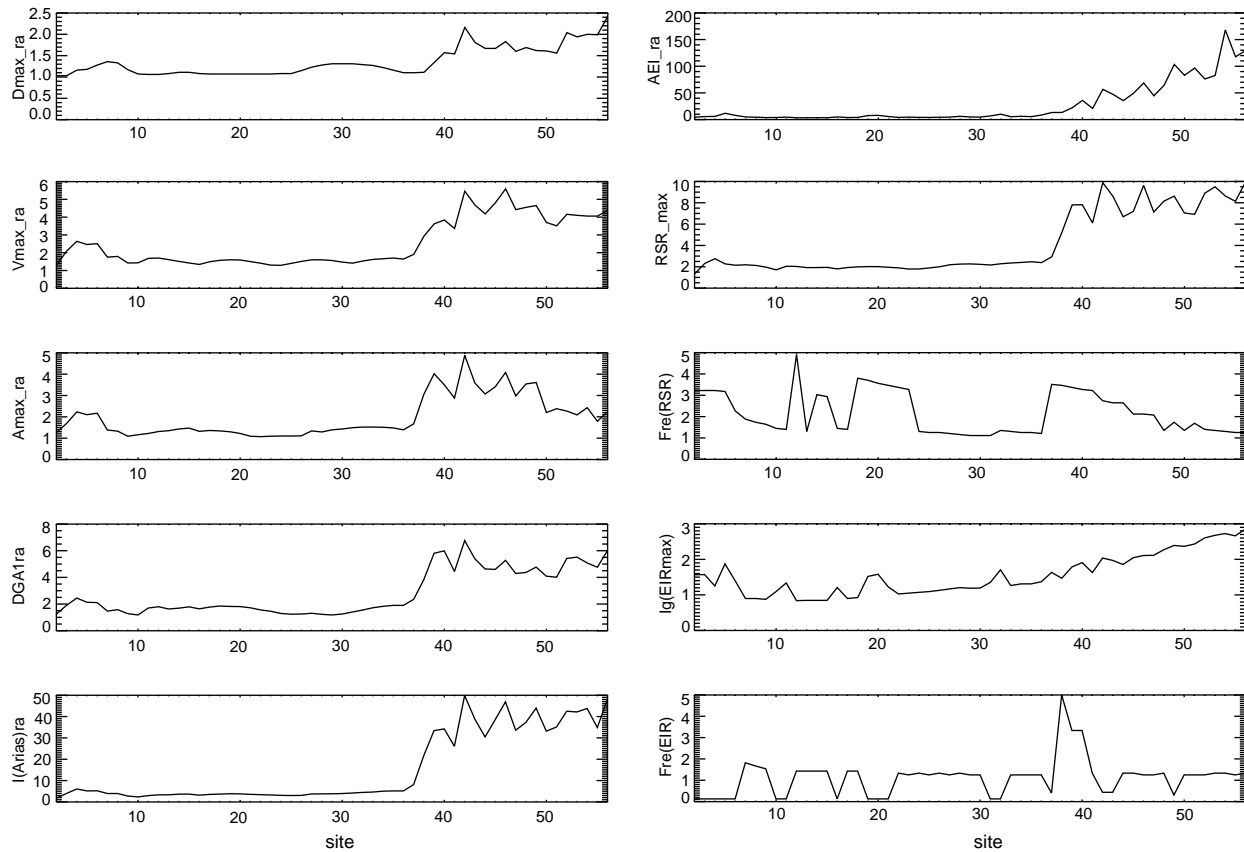


Fig. 5. Example of the variation of the considered relative ground motion parameters along a profile (the one labelled as 'p3' in Fig. 2a and b). The x-axes represent the number of the sites along the profile.

purposes of Santiago de Cuba. These results, while limited, have shown the applicability of the method. At present we have six functions three components for $RSR(f)$ and three components for $E_1R(f)$ evaluated for the 115 selected sites that can be used for classification [the same space sampling as in the case of single valued ground motion parameters is used, justified by the smooth spatial variation of $RSR(f,x)$ and $E_1R(f,x)$]. The functions are frequency sampled with 20 points uniformly distributed between 0.39 and 4.95 Hz. Six sets of values are formed, one per function and component.

5.3. Final microzoning

The process of classification of the nine sets of values results in a subdivision of the sites in groups that in general can be considered different. Seismic microzoning is characterised by generalisation and smoothing. Therefore, these groups should be as few as possible, and nearly corresponding groups should be merged together. At the end of the process every site will be characterised by nine numbers that represent the group to which it belongs in each set. This data are used as input for a new classification, and as a result a new grouping of sites is done. Each group corresponds to a quasi-uniform

behaviour of soils in terms of ground motion parameters and $RSR(f)$ and $E_1R(f)$ functions. These groups define the final microzoning.

5.4. Method of classification

For the classification of ground motion parameters and functions, as well as for the final microzoning, an extension of the non-supervised logical-combinatorial algorithms included in PROGNOSIS system [39] has been tested. The extension is due to Pico [40] and allows us the interactive selection of the similarity levels at which the partition in groups of the initial sample will be done. Two main algorithms were used: compact sets and connected components [40].

The selected algorithms start from the general conditions:

- Let the site ' j ' be the object ' O_j '. An object is described in term of variables ' $x_i(O_j)$ ', $i=1, n$.
- Let $S(O_i, O_j)$ be the similarity function between objects O_i and O_j ; $S(O_i, O_j)$ will be defined below. Two objects O_i and O_j are β_o -similar, if and only if $S(O_i, O_j) \geq \beta_o$, where β_o , the level of the classification, can be between 0 and 1.

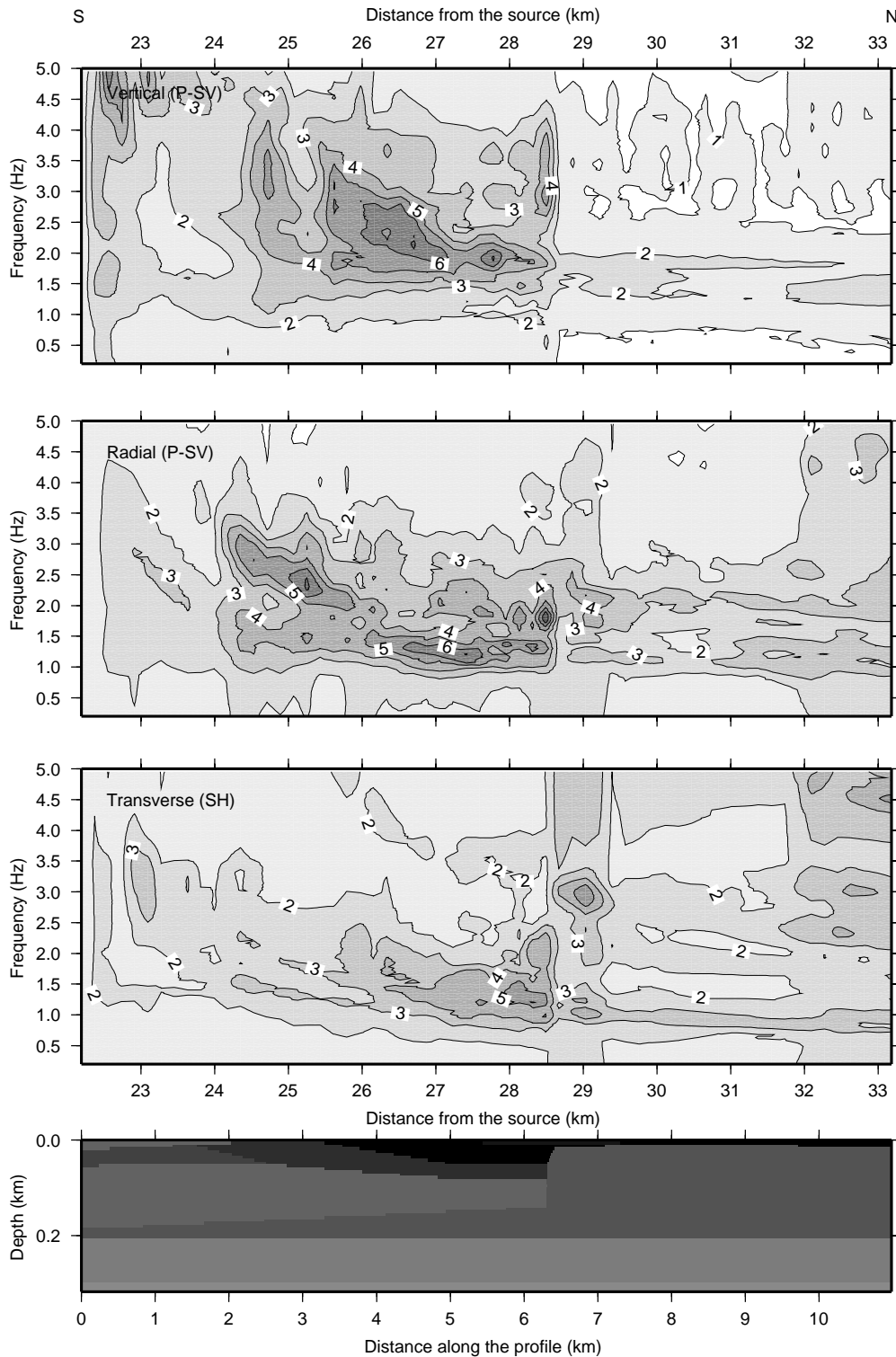


Fig. 6. Relative response spectra (RSR) for the P—SV and SH waves as a function of frequency along the profile labelled ‘pb’ in Fig. 3a and b. The uppermost 210 m of the local model along the profile is plotted below the panels of RSR. The numbers along the x-axes correspond to the epicentral distance.

- An object belongs to a connected component if all its β_o -similar objects belong to this component.
- An object belongs to a compact set if the most β_o -similar to it belongs to this set too, or if it is the most similar to another object belonging to the set.
- The compact sets or the connected components are graphically represented in a dendrogram (Fig. 8), where the different levels represent the β_o -similarity, which can be used to build groups. Selecting interactively, over this scheme, a level β_o , a particular

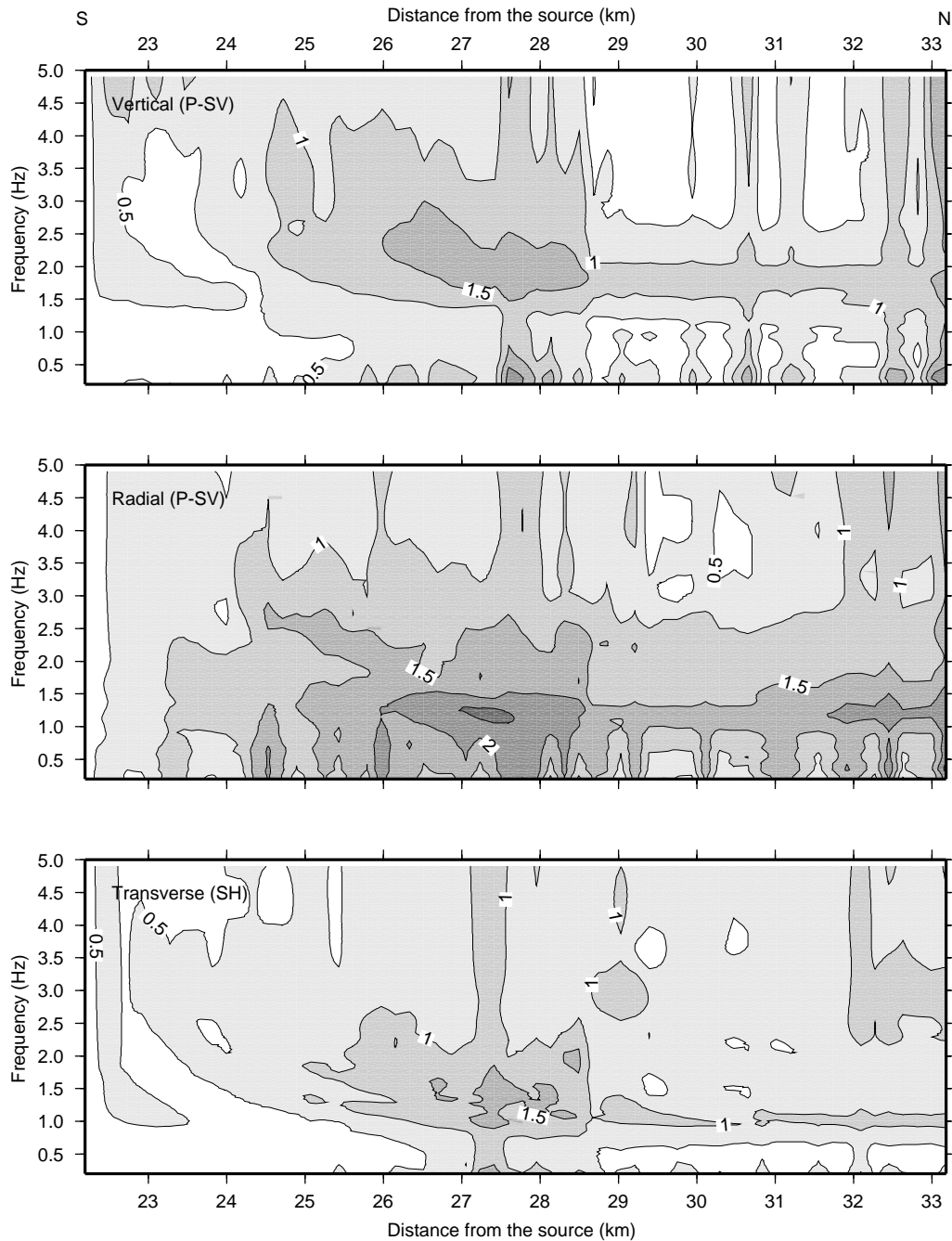


Fig. 7. Logarithm of the relative elastic energy input spectra (E_1R) of the P—SV and SH waves as a function of frequency along the profile labelled 'pb' in Fig. 3a and b. The numbers along the x-axes correspond to the epicentral distance.

partition in β_o -compact sets or in β_o -connected components can be obtained [40].

- A unique tree forms the dendrogram for the connected components, i.e. there is a β_o level such that all the objects are connected. Besides, the dendrogram for the compact sets is, in general, formed by several isolated trees; i.e. while reducing the level β_o , the number of independent groups cannot be reduced below a certain

limit. This behaviour is due to the fact that in the case of compact sets, the condition of connectivity between objects is more stringent than in the case of the connected components.

- The procedure starts by fixing the β_o level and so the β_o -compact sets or β_o -connected components are determined; then, some of the resulting groups can be

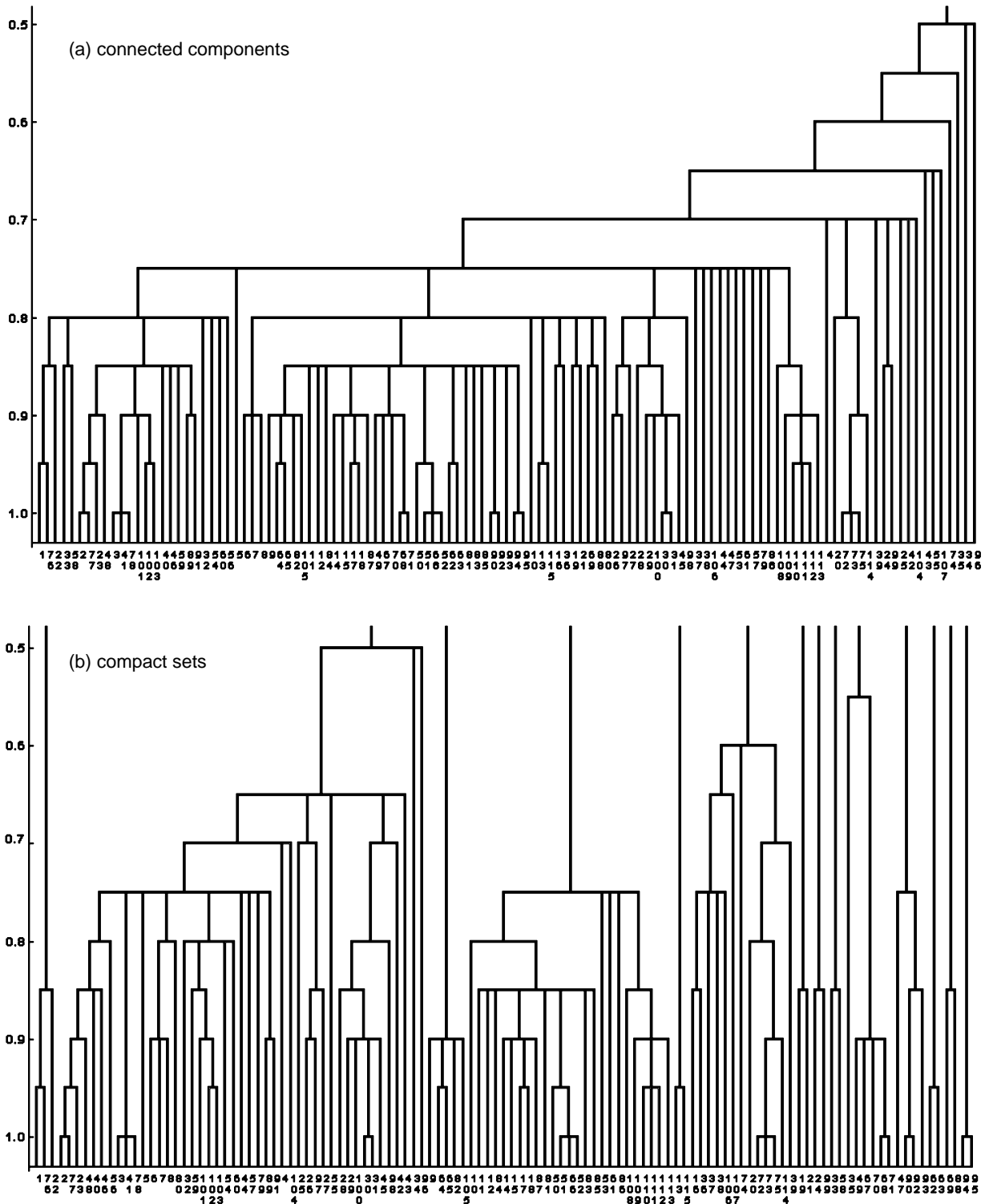


Fig. 8. Examples of the grouping of objects with the used classification algorithms. For the same input data, the grouping in connected components (a) and in compact sets (b) are shown. In the y-axes the values of the similarity function are shown, while in the x-axes the ordinal number in the input data of the objects is shown.

subdivided using additional criteria, and the average curve for each final group is calculated.

The initial settings for the classification process depend on the sample characteristics. 20 equally spaced frequency

samples, i.e. f_i , ($i = 1, 20$), are taken for the functions $RSR(f)$ and $E_I R(f)$ and correspond to the variables x_i . In the case of ground motion parameters, the variables x_i are the selected parameters for the classification ($i = 1, 3$), while for the final microzoning the variables x_i are the results of the

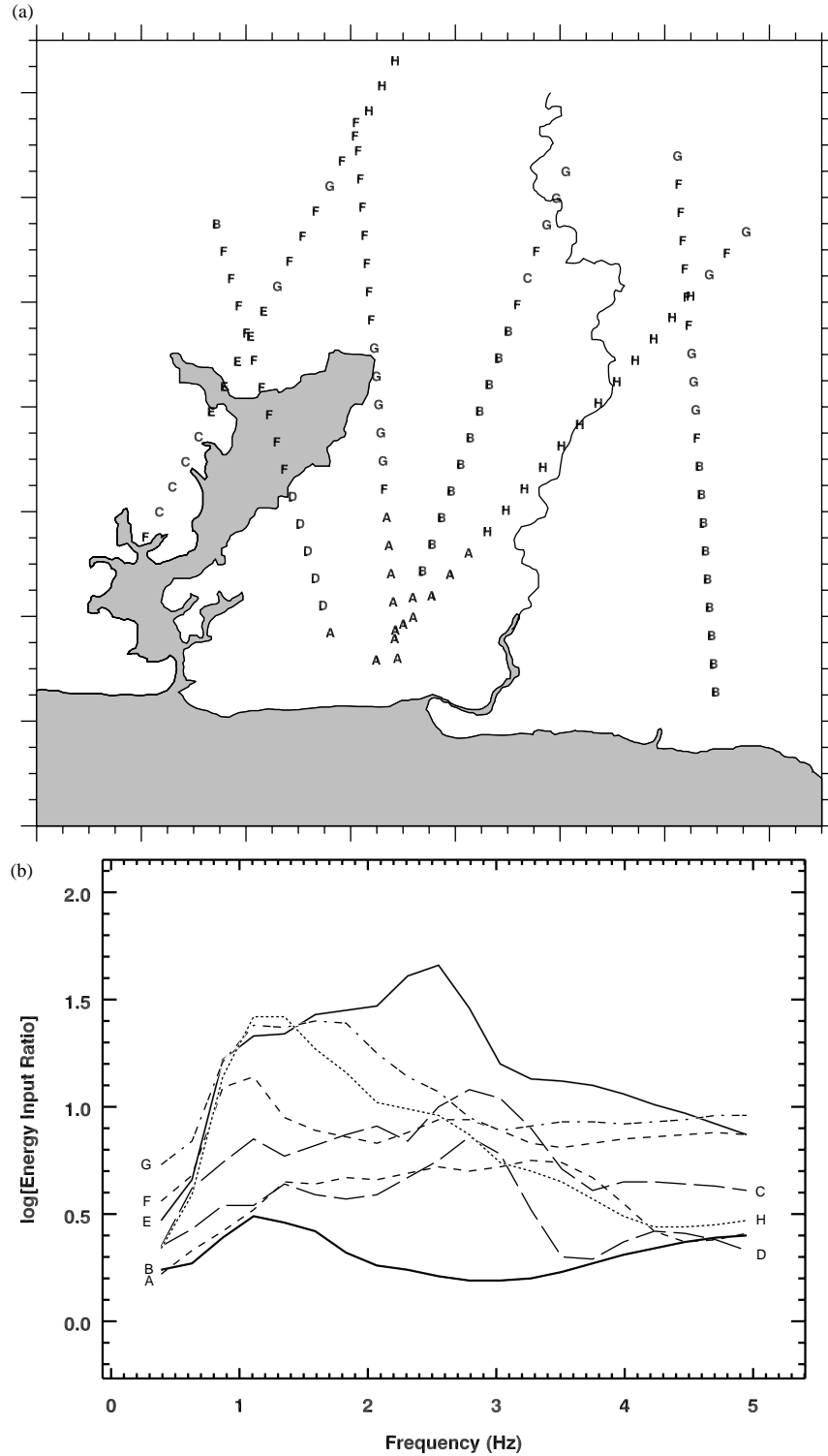


Fig. 9. Results of the classification using $\log[E_iR]$ of the transverse component of motion. (a) Map representation of the results of the classification of all the curves. The ticks on the frame of the figure are 0.5 km apart, the left-low corner has coordinates 19.945°N. and 75.897°W.; (b) Average $\log[E_iR(f)]$ curves for each of the groups.

classification of the original sets ($i=1, 9$) (integer numbers corresponding to the coding used in those classifications). The calculus of the similarity functions $S(O_i, O_j)$ is done as follows:

- In the case of connected components, used for the ground motion parameters, the comparison criterion for a variable x_r is the function C_r , defined as:

$$C_t[x_t(O_i), x_t(O_j)] = 1 - \frac{|x_t(O_i) - x_t(O_j)|}{\max(x_t) - \min(x_t)} \quad (6)$$

where $\max(x_t)$ and $\min(x_t)$ are the extremes of the variable x_t over all the objects.

- In the case of compact sets, used for RSR and E_1R curves, the comparison criterion for a variable x_t is:

$$C_t[x_t(O_i), x_t(O_j)] = \begin{cases} 1 & \text{if } |x_t(O_i) - x_t(O_j)| \leq \varepsilon_t \\ 0 & \text{elsewhere} \end{cases} \quad (7)$$

where the ε_t has been selected as $0.1 * [\max(x_t) - \min(x_t)]$

- In the case of microzoning, the values of the variables are integer numbers, and the comparison is made by means of the simple equality:

$$C_t[x_t(O_i), x_t(O_j)] = \begin{cases} 1 & \text{if } x_t(O_i) = x_t(O_j) \\ 0 & \text{elsewhere} \end{cases} \quad (8)$$

- The similarity between objects in all the cases is calculated by the formula:

$$S(O_l, O_k) = 1/n \sum_{t=1}^n C_t[x_t(O_l), x_t(O_k)] \quad (9)$$

where n is the number of considered variables and C_t the criterion defined above.

6. Results

The three sets of the $RSR(f)$ function and the three sets of the $E_1R(f)$ function have been classified in compact sets. The results of this classification are six maps with the coding of the obtained groups and the corresponding plots of the average functions for each group (an example is given in Fig. 9a and b for the transverse $E_1R(f)$). In Fig. 9a it is seen that nearly coincident sites belonging to different profiles are not always classified in the same group. This is due to the fact that waveforms in laterally varying media do not depend only on the structure under the site where they are analysed, but on the source-site path of the bi-dimensional structure (e.g. see Ref. [41]).

The three sets for the ground motion parameters have been classified in connected components. An example is given in Fig. 10 for the radial component of ground motion. In Fig. 10a a map is shown with the coding of the classification, and in Fig. 10b all the data belonging to the groups in which this set is classified are plotted.

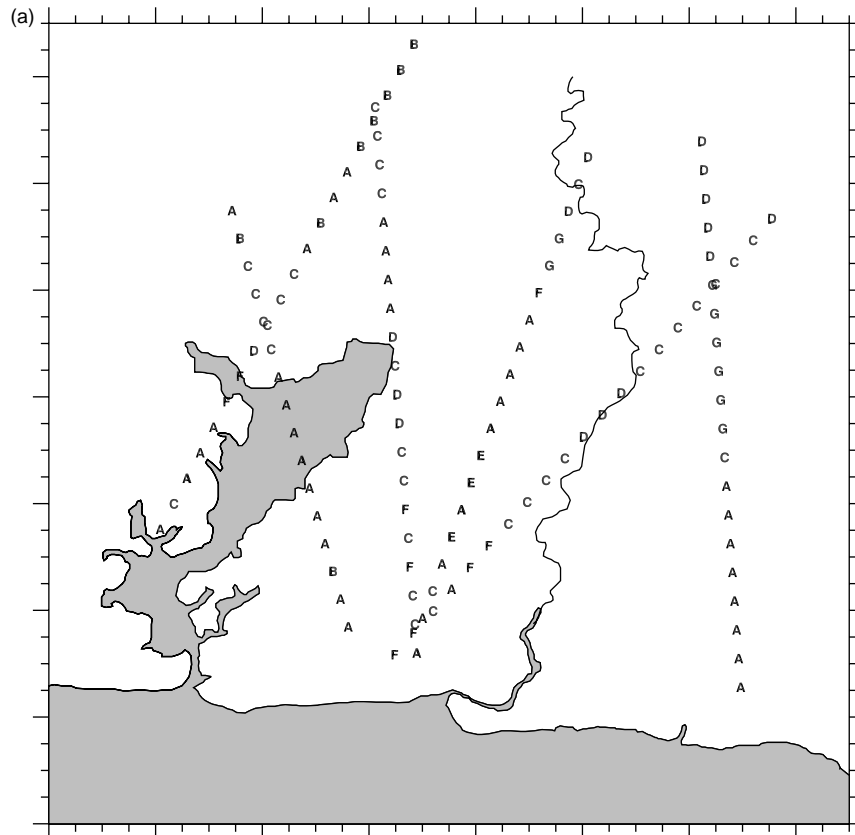


Fig. 10. Results of the classification using the ground motion parameters of the radial component of motion. (a) Map representation of the results of the classification of all the curves. The ticks on the frame of the figure are 0.5 km apart, the left-low corner has coordinates 19.945°N. and 75.897°W.; (b) plot of the groups (A–G) in which the initial sample has been classified. In the x -axis, the value one corresponds to PGVR, 2 to $f(RSR_{max})$ and three to $f(E_1R_{max})$. The y -axis units are non-dimensional for 1, and Hz for two and three.

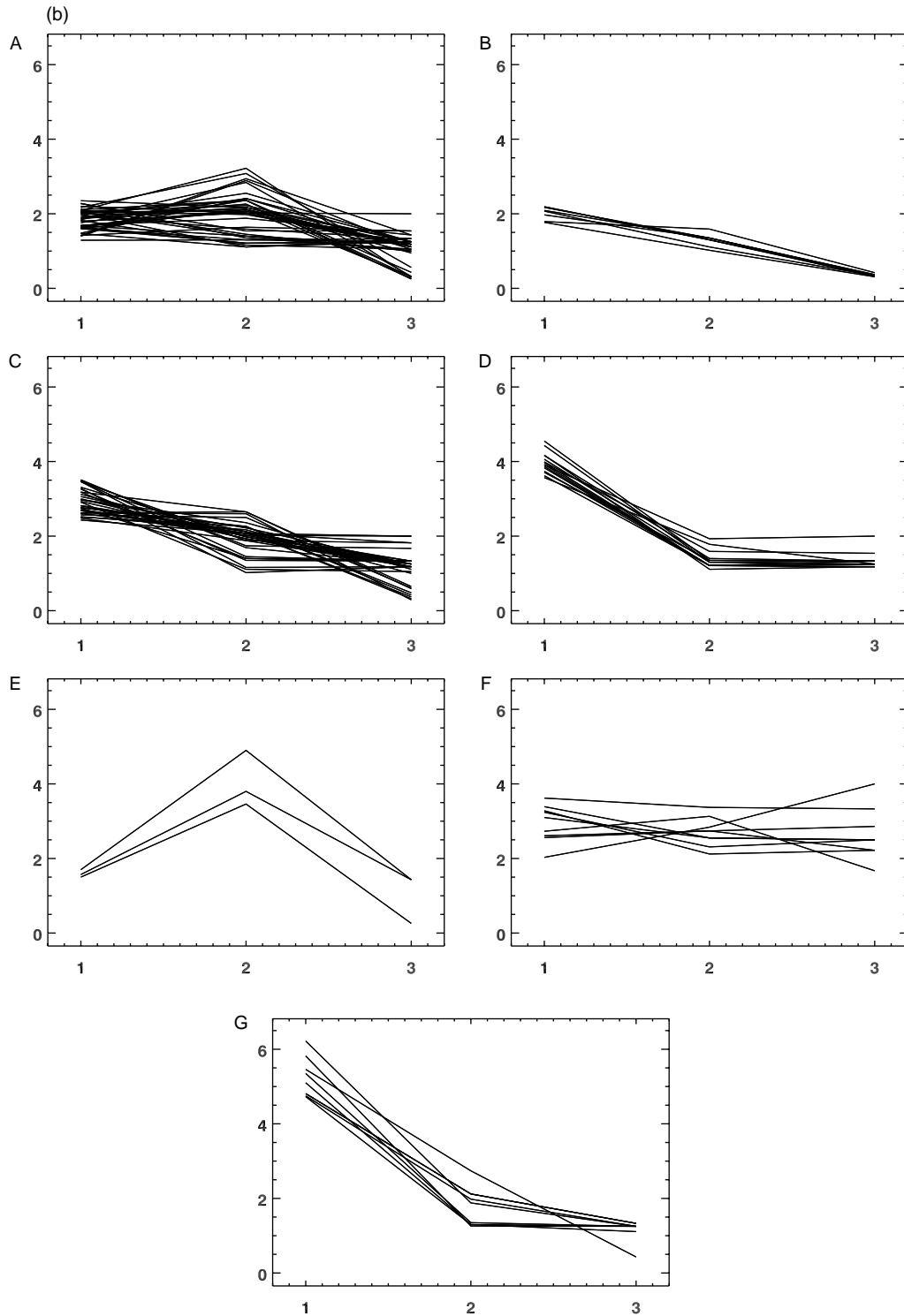


Fig. 10 (continued)

At this stage, we have nine different maps (one for each initial set of values) with a coding that represents how the particular characteristics of the ground motion vary in space. Each map could be selected to do the microzoning. We have no elements to choose the best one for doing the

microzoning, and therefore we have decided to use all the maps together. For doing so, the coding defined in each of the nine maps is considered as a new initial sample to be classified in connected components too, leading to a map with the final microzoning coding (Fig. 11).

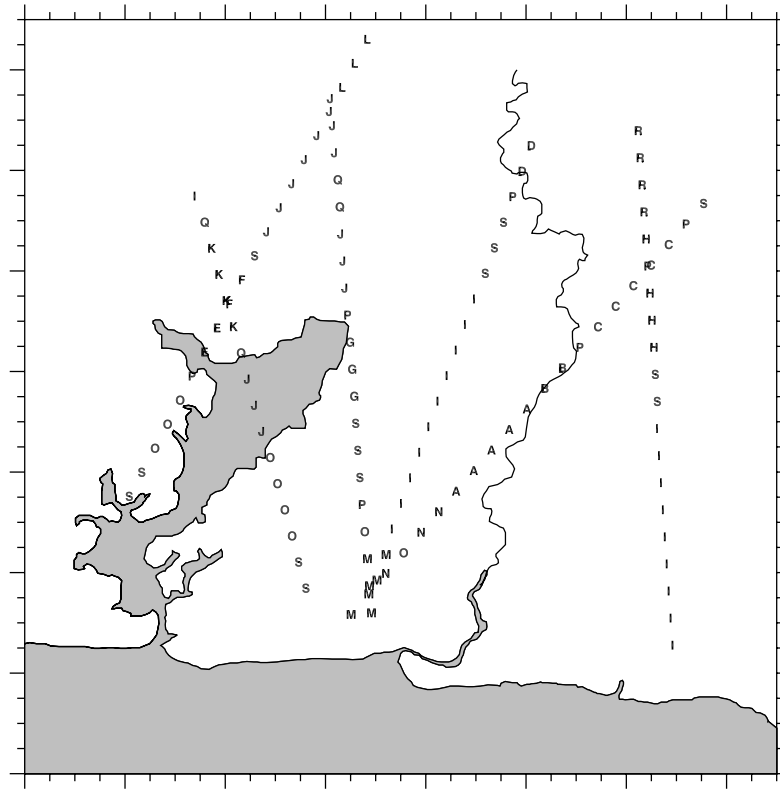


Fig. 11. Final classification. Map representation of the quasi-homogeneous groups to which the selected sites belong. The ticks on the frame of the figure are 0.5 km apart, the left-low corner has coordinates 19.945°N. and 75.897°W.

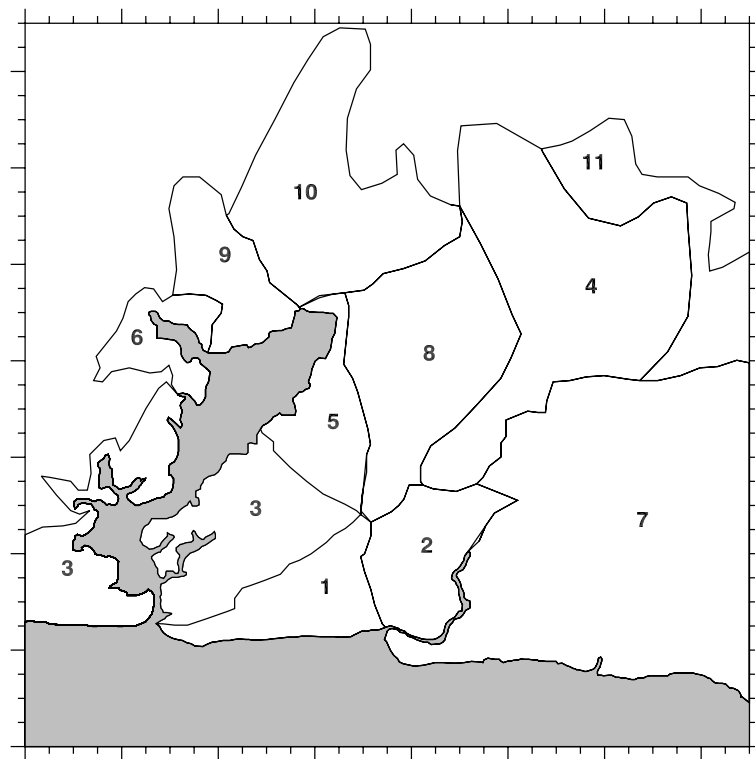


Fig. 12. Microzoning scheme of Santiago de Cuba. The different zones are delimited combining geological information and the result of the classification. The ticks on the frame of the figure are 0.5 km apart, the left-low corner has coordinates 19.945°N. and 75.897°W.

7. Discussion

The influence of local soil conditions on earthquake signals is clearly seen from the signals shown in Fig. 4. The relative ground motion parameters, shown in Fig. 5, give a good characterisation of the influence of soil properties on earthquake ground motion. The complexity of the problem is evident from the fact that the signals vary not only from one profile to another, but for each profile, from one component of motion to the other. The $RSR(f,x)$ and $\log[E_1R(f,x)]$ plots (Figs. 6 and 7, respectively) in a gross way show the same general characteristics.

The problem of selecting the best way to characterise the earthquake seismic ground motion is not solved until now. The analysis of the relative ground motion parameters and RSR and E_1R functions evidences the impossibility to select one of them for microzoning purposes; therefore our decision to make a classification using all the data. The classification had to be done in

two parts: (a) each data set (three RSR, three E_1R , three ground motion parameters) has been independently classified; (b) the results of step (a) have been used as input for another classification that leads to the final microzoning. The maps of the kind presented in Figs. 9a and 10a cannot be combined by means of a straightforward procedure. Again, the way for solving the problem has been to classify these preliminary results. Rather than the spatial distribution of a single parameter, as is usual in microzoning maps, the map of Fig. 11 shows the spatial distribution of sites with quasi-homogeneous behaviour. Each group identified after the final classification is not characterised by a common value of a given ground motion parameter, taken as a criterion for microzoning. Instead, the sites belonging to each group are characterised by a given degree of similarity among the nine initially classified sets of values that describe the ground-motion characteristics. The sites have similar, but not equal behaviour in

Table 2

Average values, for the three components of motion, of the relative parameters defined in formulae 1–5 (ratio between the values obtained considering the 2D model—soil—and those obtained for the reference model—bedrock) in the sites placed into the zones delimited in Fig. 12

Zone	PGDR	PGVR	PGAR	DGAR	$I_A R$	RSR_{max}	AE_1R	$\log(E_1R)_{max}$
(a) Radial								
1	1.44	2.34	1.87	1.99	5.23	2.62	6.46	1.02
2	1.52	2.73	2.01	2.63	9.44	4.13	11.30	1.29
3	1.43	1.91	1.47	1.78	5.60	2.66	9.73	1.40
4	2.06	3.96	2.79	5.16	44.44	8.71	75.19	2.45
5	1.93	3.04	1.89	3.35	23.82	5.53	43.75	1.92
6	1.69	3.25	2.64	3.19	28.59	5.78	28.66	1.74
7	1.49	2.20	1.65	1.87	6.33	2.59	8.35	1.15
8	1.25	2.03	1.83	2.37	10.06	3.21	10.53	1.20
9	1.21	2.44	2.17	2.33	16.85	3.57	33.64	1.95
10	1.43	2.35	2.17	2.38	15.95	3.69	53.43	2.12
11	1.95	3.84	2.41	4.98	41.17	7.22	92.93	2.72
(b) Transverse								
1	1.23	1.63	1.56	2.09	4.34	2.84	2.73	0.77
2	1.24	1.18	1.50	2.34	6.19	3.71	2.88	1.08
3	1.29	1.71	1.42	2.19	5.43	2.64	4.14	0.98
4	1.32	1.96	1.90	4.56	23.29	6.13	11.83	1.75
5	1.18	2.35	1.71	3.10	15.38	3.84	10.81	1.27
6	1.44	1.99	2.50	3.88	25.53	6.37	10.48	1.69
7	1.14	1.44	1.17	1.79	3.80	2.30	2.39	0.71
8	1.14	1.31	1.45	1.86	5.13	2.26	2.74	0.77
9	1.35	2.32	2.33	2.80	13.14	3.46	9.80	1.34
10	1.23	1.59	2.06	2.91	12.55	4.16	6.53	1.30
11	1.37	2.68	1.84	5.64	21.88	6.04	13.25	1.77
(c) Vertical								
1	1.12	1.65	1.84	3.17	7.18	4.77	3.22	1.06
2	0.95	1.59	1.43	2.43	5.58	2.97	3.15	0.85
3	0.96	1.34	1.34	2.60	8.81	3.23	5.03	1.11
4	1.00	1.69	1.71	4.29	23.91	5.19	11.75	1.60
5	0.87	1.65	1.58	4.21	23.40	5.10	12.07	1.44
6	0.89	1.11	1.14	2.57	13.44	3.80	6.03	1.19
7	0.94	1.07	0.90	1.69	3.46	2.28	2.16	0.73
8	0.88	1.17	1.19	1.79	3.49	2.35	2.31	0.71
9	0.86	0.90	0.84	1.74	6.41	2.39	7.68	1.27
10	0.91	1.01	0.79	1.83	7.70	2.08	13.01	1.49
11	1.04	1.18	1.18	2.22	15.76	3.41	14.99	1.62

Being relative values, they are non-dimensional.

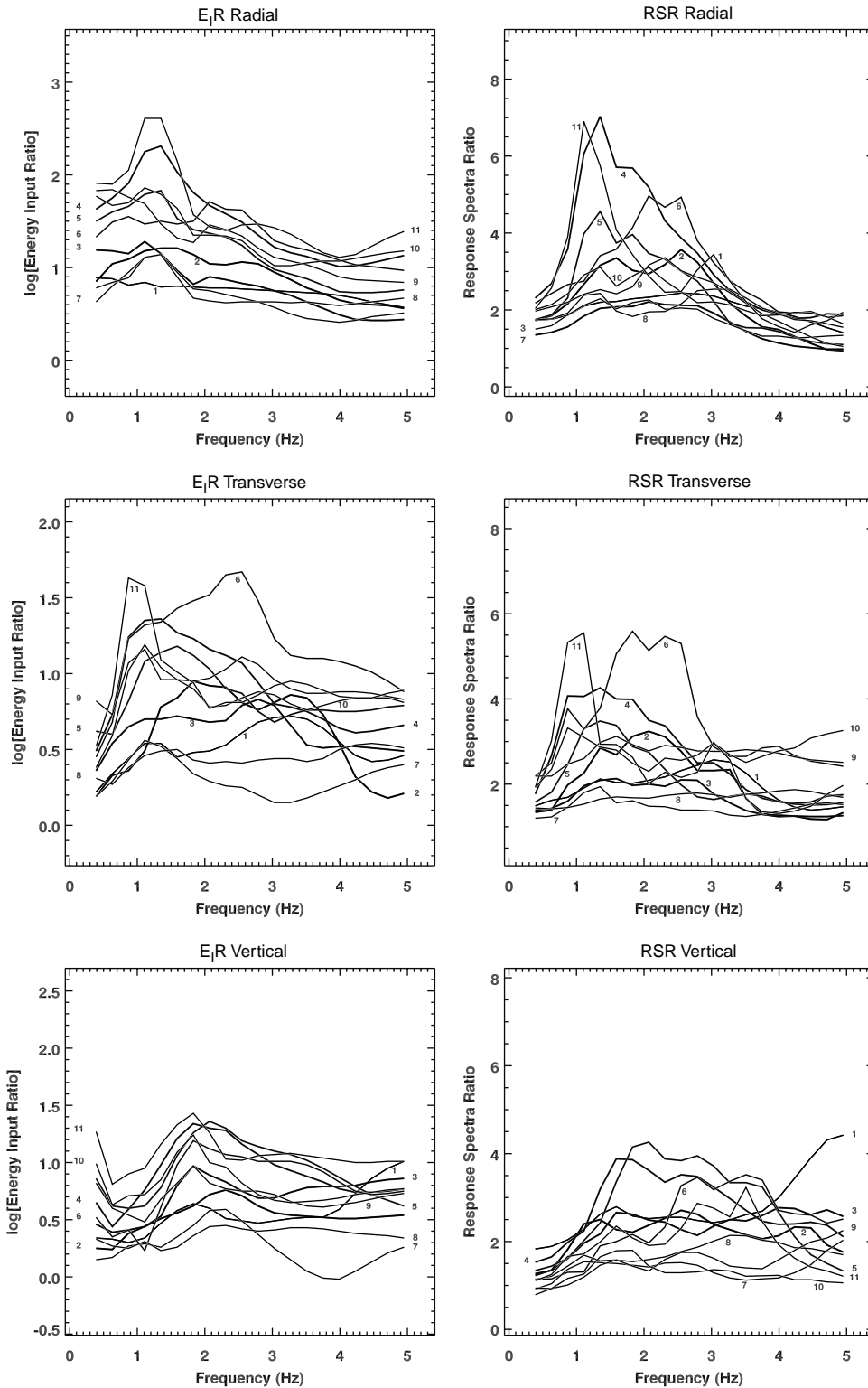


Fig. 13. Average curves of $RSR(f)$ and $\log[E_1R(f)]$ (radial, transverse and vertical component of motion) corresponding to each of the zones of the microzoning scheme. They are labelled accordingly to the numbers in Fig. 12.

response to seismic load. The degree of similarity used to define the groups is measured by the similarity between the objects defined in Eqs. (8) and (9). The average similarity of the sites represented in the map of

Fig. 11 is 0.66, which means, according with Eq. (9), that six out of the nine variables are equal. Nevertheless, for some of the groups shown in Fig. 11 (those identified with letters A–L) the similarity is 0.77, which

corresponds to seven equal variables, and there is only one group with similarity of 0.55 (identified with letter S) that corresponds to only five equal variables.

Seismic microzoning requires a division in zones, of the study region. If we analyse the site spatial distribution in Fig. 11, it is evident that for the studied area it is not possible to produce a map, but if we add other information to our results we can make a microzoning scheme. Our choice has been to use the geological map of Santiago de Cuba basin of Medina et al. [32] (see Fig. 3a) and the microzoning scheme proposed in [11]. In Fig. 12 we present the final microzonation. It has been constructed by tracing the boundaries between zones following, as close as possible, the limits between the geological formations, and avoiding to make additional generalisations of the results of classification. For each zone of Fig. 12, we calculated average single valued quantities (see Table 2) and average $RSR(f)$ and $E_I R(f)$ functions (Fig. 13), obtained from the signals associated with the sites belonging to each zone.

8. Conclusions

Earthquake ground motion has been characterised by means of several relative (soil/bedrock) single valued quantities (PGDR, PGVR, PGAR, DGAR, I_{AR} , etc.), by the response spectra ratio $RSR(f)$ and by the elastic energy input ratio $E_I R(f)$ (defined in this paper). The parameters have been extracted from synthetic data. No calibration with real data could be done, since strong-motion observations are not available in the study area. This lack of data has been discussed in [19], where a comparison with two microzoning maps obtained by other authors using different methodologies is discussed. Even if with the synthetic modelling it is easy to consider different earthquake scenarios, a single one has been taken into account, since Santiago de Cuba is placed in a region where the plate boundary (North America—Caribbean) is very narrow and well defined, and no deep earthquakes are observed.

The seismic microzoning has been done by classifying these data using two logical combinatory algorithms: connected components and compact sets [40]. Data were sampled at 115 sites distributed along six profiles that sample the study area.

The classification process has been accomplished in two steps. The original nine data sets (RSR and $E_I R$ functions, and single-valued ground motion parameters, for the different components of motion—radial, transverse and vertical) are classified at first. In this way, the spatial distribution of the soil behaviour as a function of the component of motion is obtained. The results of this classification are used as input for a further classification to define the spatial distribution of the sites with a quasi-homogeneous integral ground motion behaviour. The

latter classification is combined with the geological surface data available to produce a microzoning scheme for Santiago de Cuba basin.

References

- [1] Kanai K, Tanaka T. Measurement of the microtremor. Bull Earthquake Res Inst 1954;32:199–209.
- [2] Medvedev SM. Engineering seismology (in Russian). Moscow: Nauka; 1962.
- [3] Medvedev SM. Seismic microzoning (in Russian). Moscow: Nauka; 1977.
- [4] Pavlov OY, editor. Seismic microzoning (in Russian). Moscow: Nauka; 1984.
- [5] Borcherd RD. Effects of local geology near San Francisco Bay. Bull Seismol Soc Am 1970;60:29–61.
- [6] Murphy JR, Hewlett RA. Analysis of seismic response in the city of Las Vegas, Nevada: a preliminary microzonation. Bull Seismol Soc Am 1975;65:1575–98.
- [7] Hays WW. Procedures for estimating earthquake ground motions. Geological survey professional paper. 1114. Washington, USA: Government Print Office; 1980.
- [8] Nakamura, K. Inferences of seismic responses of surficial layer based on microtremor measurement (in Japanese). Quarterly Report on Railroad Research, Vol. 4, Railway Technical Institute; 1989. p. 18–27
- [9] Bard P. Microtremor measurements: a tool for site effect estimation?. In: Irikura, Kudo, Okada, Sasatani, editors. The effects of surface geology on seismic motion, 1999. p. 1251–79.
- [10] Fäh D, Iodice C, Suhadolc P, Panza GF. Application of numerical simulations for a tentative seismic microzonation of the city of Rome. Ann Geofis 1995;38:607–16.
- [11] Alvarez L, García J, Vaccari F, Panza GF, Gonzalez B, Reyes C, et al. Ground motion zoning of Santiago de Cuba: an approach by SH waves modelling. Pure Appl Geophys 2004;161:1041–59.
- [12] Panza GF, Romanelli F, Vaccari F. Seismic wave propagation in laterally heterogeneous anelastic media: theory and applications to the seismic zonation. Advances in geophysics no. 43. London: Academic Press; 2000 p. 1–95.
- [13] Panza GF, Alvarez L, Aoudia A, Ayadi A, Benhallou H, Benouar D, et al. Realistic modeling of seismic input for megacities and large urban areas (the UNESCO/IUGS/IGCP project 414). Episodes 2002; 25:160–84.
- [14] Panza GF. Synthetic seismograms: the Rayleigh waves modal summation. J Geophys Res 1985;58:125–45.
- [15] Panza GF, Suhadolc P. Complete strong motion synthetics. In: Bolt BA, editor. Strong motion synthetics, computational techniques 4. Orlando: Academic Press; 1987. p. 153–204.
- [16] Florsch N, Fäh D, Suhadolc P, Panza GF. Complete synthetic seismograms for high-frequency multimode SH-waves. Pure Appl Geophys 1991;136:529–60.
- [17] Fäh, D., 1992. A hybrid technique for the estimation of strong ground motion in sedimentary basins. PhD Thesis, Nr. 9767, Swiss Fed. Inst. Technology, Zurich.
- [18] Fäh D, Iodice C, Suhadolc P, Panza GF. A new method for the realistic estimation of seismic ground motion in megacities, the case of Rome. Earthquake Spectra 1993;9:643–68.
- [19] Alvarez L, Vaccari F, Panza GF, González BE. Modelling of ground motion in Santiago de Cuba City from earthquakes in Oriente fault seismic zone. Pure Appl Geophys 2001;158:1763–82.
- [20] González, BE, Mirzoev, KM, Chuy, T, Golubiatnikov, VL, Lyskov, LM, Zapata, JA, Alvarez, H. Microzonación sísmica de la ciudad de

- Santiago de Cuba, Comunicaciones Científicas sobre Geofísica y Astronomía No. 15, Instituto de Geofísica y Astronomía, Academia de Ciencias de Cuba; 1989.
- [21] González BE. Estimación del efecto sísmico en la ciudad de Santiago de Cuba. Tesis en opción al grado de Candidato a Doctor en Ciencias Físicas, Instituto de Geofísica y Astronomía, La Habana; 1991.
- [22] Zapata JA. Utilización de variantes metodológicas de microzonificación sísmica en la ciudad de Santiago de Cuba. In: Zapata JA, editor. Red de estaciones e investigaciones sismológicas en Cuba. La Habana: Editorial Academia; 2000. p. 88–112.
- [23] García J, Arango E, Zapata JA, Oliva J, González B, Fernández B, Chuy T, Reyes C, Monnar O. Mapa de riesgo sísmico de la ciudad de Santiago de Cuba. Report, Centro Nacional de Investigaciones Sismológicas, Santiago de Cuba; 2002.
- [24] Uang CM, Bertero VV. Evaluation of seismic energy in structures. *Earthquake Eng Struct Dyn* 1990;19:77–90.
- [25] Decanini L, Mollaioli F. Formulation of elastic earthquake input energy spectra. *Earthquake Eng Struct Dyn* 1998;27:1503–22.
- [26] Panza GF, Cioflan C, Kouteva M, Paskaleva I, Romanelli F, Marmureanu G. An innovative assessment of the seismic hazard from Vrancea intermediate-depth earthquakes: case studies in Romania and Bulgaria. *ICTP Preprint No. IC/2002/6*; 2002.
- [27] Decanini L, Mollaioli F. An energy-based methodology for the assessment of seismic demand. *Soil Dyn Earthquake Eng* 2001;21: 113–37.
- [28] Arriaza G. Nuevos enfoques en la interpretación y procesamiento de las ondas refractadas para el estudio del basamento de Cuba. Tesis presentada en opción al grado científico de Doctor en Ciencias Geológicas. La Habana; 1998.
- [29] Orihuela N, Cuevas JL. Modelaje sismogravimétrico de perfiles regionales del Caribe central, *Revista Ingeniería, Universidad Central de Venezuela*. In: *Revista Ingeniería, Universidad Central de Venezuela*, vol. 8, 1993. p. 55–73.
- [30] Van der Hilst RD. Tomography with P, PP and pP delay-time data and the three-dimensional mantle structure below the Caribbean region. PhD Thesis. University of Utrecht; 1990.
- [31] Moreno B, Grandison M, Atakan K. Crustal velocity model along the southern Cuban margin: implications for the tectonic regime at an active plate boundary. *Geophys J Int* 2002;150:1–14.
- [32] Medina A, Escobar E, Ortiz G, Ramírez M, Díaz L, Mónico F, Montejo N, Diéguez H, Guevara T, Acosta J. Reconocimiento geólogo-geofísico de la cuenca de Santiago de Cuba, con fines de riesgo sísmico. Report, Empresa Geominera de Oriente, Santiago de Cuba; 1999.
- [33] Ishihara K. (chairman). The Technical Committee for earthquake Geotechnical Engineering (TC-4) of the International Society for Soil Mechanics and Foundation Engineering, Manual for Zonation on Seismic Geotechnical Hazards. The Japanese Society of Soil Mechanics and Foundation Engineering; 1993.
- [34] Berge Thierry C, Lussou P, Hernández B, Cotton E, Gariel JC. Computation of the strong motions during the 1995 Hyogoken-Nambu earthquake, combining the k-square spectral source model and the discrete wavenumber technique. In: *Proceedings of the Second International Symposium on the Effects of Surface Geology on Seismic Motion, Yokohama, Japan, 1–3 December, 1998*; Volume 3, *The Effects of Surface Geology on Seismic Motion, Recent Progress and New Horizon on ESG Study, 1999*. p. 1414–1424.
- [35] Panza GF, Vaccari F, Costa G, Suhadolc P, Fäh D. Seismic input modelling for zoning and microzoning. *Earthquake Spectra* 1966;12: 529–66.
- [36] Gusev AA. Descriptive statistical model of earthquake source radiation and its application to an estimation of short period strong motion. *Geophys J Roy Astron Soc* 1983;74:787–800.
- [37] Aki K. Strong motion seismology. In: Erdik MÖ, Toksöz MN, editors. *Strong ground motion seismology, NATO ASI series. Series C: mathematical and physical sciences*, vol 204. Dordrecht: Reidel Publishing Company; 1987. p. 3–41.
- [38] Norma Cubana NC 46: 1999. Construcciones sismo resistentes. Requisitos básicos para el diseño y construcción, 3. Edición ICS: 91.080; 91.120.25. Oficina Nacional de Normalización, Ciudad de La Habana; 1999.
- [39] Ruiz J, Pico R, López R, Alaminos C, Lazo M, Baggiano M, Barreto E, Santana A, Alvarez L, Chuy T. PROGNOSIS y sus aplicaciones a las geociencias. In: *IBERAMIA-92, III Congreso Iberoamericano de Inteligencia Artificial, Memorias*. México: LIMUSA, 1992; p. 561–86.
- [40] Pico R. Determinación del umbral de semejanza β_0 para los algoritmos de agrupamiento lógico-combinatorios, mediante el dendrograma de un algoritmo jerárquico. *SIARP'99, IV Simposio Iberoamericano de Patrones. Memorias, 1999*, p. 259–265.
- [41] Triantafyllidis P, Suhadolc P, Hatzidimitriou D. Influence of source on 2D site effects. *Geophys Res Lett* 2002;29(6):13.